Joint Impedance Spectroscopy and Fractography Data Analysis of Ceria Doped Scandia Stabilized Zirconia Solid Electrolyte modified by powder types and sintering temperature

Iryna V. Brodnikovska[a*], Mykola M. Brychevskyi[a], Yehor M. Brodnikovskyi[a], Dmytro M. Brodnikovskyi[a], Oleksandr D. Vasylyev[a], Alevtina L. Smirnova[b]

[a] *Laboratory for SOFC, Frantsevych Institute for Problems of Material Science, Krszhizhanovskoho Street, 3, Kyiv 03860, Ukraine*

[b] *South Dakota School of Mines and Technology, 501 E St Joseph St, Rapid City, South Dakota 57701, USA*

Brodnikovska@i.ua

Keywords: *non-Debye relaxation; grain resistance; boundary resistance; zirconia powders; sintering temperature.*

Parameters of the non-Debye relaxation in the 10Sc1CeSZ solid electrolyte made of various types of ZrO_2 powder stabilized with 10-mol.% Sc_2O_3 and 1-mol.% CeO_2 were studied. The influence of powder properties and their sintering temperatures on the impedance spectra is analyzed. In regard to electrical response, the polycrystalline ceramic electrolytes may be considered as a single-phase or a two-phase material consisting of a grain bulk and a boundary. In many cases, the boundary resistance is independent practically on dopants and their distribution across the powders and sintering temperatures. The powder compositions suitable for an electrolyte and electrodes are specified.

Introduction

Currently, a number of successful SOFC projects resulted in significantly higher efficiency at lower temperatures of operation and long-term endurance. As an example, the SOFCs made at the Energy Center of the Netherlands demonstrate high efficiency at 600°C. Duration of reliable operation of SOFCs made by Research Center Juelich is more than 70 000 h at 700°C. However, the SOFC development requires further structural optimization in order to prevent their premature degradation. It is envisaged, that structurally optimized and produced from the chemically stable high temperature materials, the advanced SOFCs would be able to operate for at least 25 years.

In this paper cubically stabilized zirconia (ZrO_2) with 10 mol.% scandia dopant (10ScSZ) and additionally stabilized by CeO_2 (1 mol. %) (10Sc1CeSZ) SOFC electrolyte is investigated as one of the most promising highly ionic

conducting and long-term stable materials [1-6] nowadays.

It is important to note that different manufacturing approaches of 1Ce10ScSZ powder, in particular co-precipitation [7], sol-gel [8], solid-phase synthesis [9], polymeric precursor method [10] significantly effect the initial properties of the powders. To produce 1Ce10ScSZ ceramic electrolyte, it is necessary to use well-dispersed highly powders with high ability for sintering resulting in high oxygen conductivity and essential densification.

The advancements in SOFC performance optimization require specific knowledge on contributions of each of the SOFC components that can be achieved by using impedance spectroscopy. Numerous interfaces namely boundaries between grains and subgrains are particularly important for understanding of the electrochemical and mechanical properties of the polycrystalline ceramic electrolytes.

In this paper, the influence of the grain and subgrain boundaries on electrical conductivity of the 1Ce10ScSZ electrolyte is considered. The required variety of the structural boundaries – grains and their subgrains – are investigated for three types of the 1Ce10ScSZ zirconia powders different in terms of their morphological properties, amount and distribution of the residual impurities across and along the particles, and the temperatures of their sintering.

Theory block

For the non-destructive investigation of fuel cell materials, the method of impedance spectroscopy (IS) is usually applied, which allows to distinguish contributions of microstructural components to the overall conductivity of the cell [11]. The alternating current electrical data of the SOFC ceramics in complex coordinates allows to distinguish two types of polarization processes with either ideal (Debye) or non-ideal (non-Debye) representation [12].

The ideal (Debye) type response, representing dipole polarization, is observed mainly in polar liquid dielectrics. In this case, the complex dielectric permittivity is described by equation (1).

$$\varepsilon^*(\omega) = \varepsilon_\infty + \frac{\varepsilon_0 - \varepsilon_\infty}{1 + j\omega\tau} = \varepsilon' - j\varepsilon'' \quad , \quad (1)$$

where ε_∞ - permittivity at the high frequency limit, ε – static permittivity at direct current conditions ($f \to 0$ Hz), and τ - relaxation time. In ideal case, the real and imaginary parts of the impedance in a complex coordinates give a semicircle with the center on the *x*-axis.

The non-Debye type responses can be visualized in a complex plane by either the skewed semicircle or the semicircle with the center below the real axis. The dielectric response of solid-state materials with ionic polarization is described with Cole-Cole (C-C), Davidson-Cole (D-C) and Havriliak-Negami (H-N) equations [11-13].

Cole-Cole relaxation

The model gives the semicircle with the centre that is below the real axis. The depression angle (θ) is estimated as an angle between the *x*-axis and the diameter of the skewed semicircle (**Figure 1**). The Cole-Cole model is described by equation (2):

$$\varepsilon^*(\omega) = \varepsilon_\infty + \frac{\varepsilon_0 - \varepsilon_\infty}{1 + (j\omega\tau_0)^\alpha}, \quad (2)$$

where the exponent α ranges in-between 0 and 1. The depression angle (θ) can be found from **Figure 1** as:

$$\theta = \text{atan}\left(\frac{\Delta y}{R/2}\right). \quad (3)$$

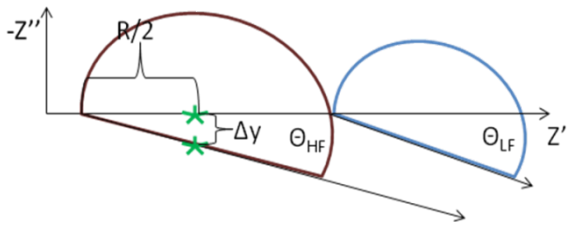

Figure 1. The impedance in a complex plane in a case of Cole-Cole relaxation model [14].

Thus, we can set the depression parameter *h*, which is given by:

$$h = \frac{\theta}{\pi/2} = \frac{2\theta}{\pi} \quad (4)$$

$$1 - h = \alpha \quad (5)$$

At $\Theta \to 0$ and $\alpha \to 1$ the Cole-Cole equation represents the Debye model.

Davidson-Cole relaxation

The Davidson-Cole model describes the skewed nature of the relaxation curve (**Figure 2**) which is represented by the following equation:

$$\varepsilon^*(\omega) = \varepsilon_\infty + \frac{\varepsilon_0 - \varepsilon_\infty}{(1 + j\omega\tau_0)^\beta}. \quad (6)$$

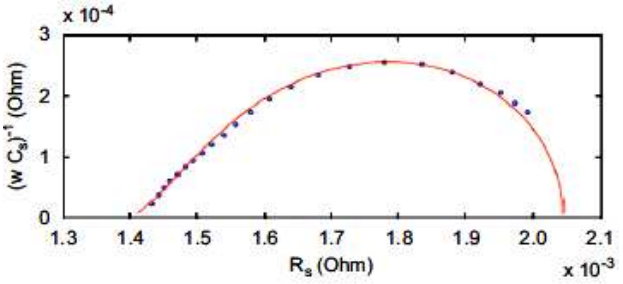

Figure 2. Davidson-Cole representation of the Ni-Cd battery via impedance plot [12].

For the ideal Debye model, the relaxation time τ_0 at the maximum of the real impedance values is determined as a multiple of resistance and capacitance: $\tau_0 = 1/\omega = RC$. The time constant in the Davidson-Cole representation is not equal to the conventional $\omega\tau = 1$ at the peak as in the Debye model. Due to the skewed shape of the impedance plot, the correction factor is defined as Z'_{PF}/Z''_{PF}, where PF is a peak frequency:

$$C = \frac{1}{R\omega_{PF}}\left(\frac{Z'_{PF}}{Z''_{PF}}\right), \quad (7)$$

$$\varphi_{PF} = a\tan\left(\frac{Z'_{PF}}{Z''_{PF}}\right), \quad (8)$$

$$\beta = \frac{\pi}{2\varphi_{PF}} - 1. \quad (9)$$

The exponent β reflects the difference in relaxation times of the system components.

It is important to note that the fitting angle θ and the exponent β might be different for low- and high-frequency semicircles. The increasing degree of sample heterogeneity with higher yttria content leads to the increasing values of β.

Havrilyak-Negami relaxation

If the impedance representation of the system in a complex plane depicts a skewed semicircle with the center below the real axis, the Havriliak-Negami equation is used to model the plot:

$$\varepsilon^*(\omega) = \varepsilon_\infty + \frac{\varepsilon_0 - \varepsilon_\infty}{(1 + (j\omega\tau_0)^\alpha)^\beta}, \quad (10)$$

where the α and β exponents can be found as it was shown above (Equations 5 and 9).

The above mentioned impedance approaches are considered for the SOFC electrochemical and materials characterization. But still most of SOFC's studies elide the aspect that in the vast majority of real SOFC materials only "fuzzy" ranges of dispersion are observed and tend to use a constant phase element (CPU) in place of a capacitor to compensate for non-homogeneity in the system. Therefore there is a lack of information according to the relaxation parameters in ceramic materials.

Experimental part

10Sc1CeSZ ceramics (1-mol.% CeO_2 – 10-mol.% Sc_2O_3 – 89-mol.% ZrO_2) was made of three types of powder with the same chemical composition, but using different initial raw materials and synthesis conditions resulting in different morphology, impurities composition, and impurities distribution. The Type I powder (Vilnohirsk Mining & Metallurgical Plant and Zirconia Ukraine Ltd., Ukraine) was made by co-precipitation technique, Type II powder (DKKK, Japan) was produced by the hydrothermal synthesis, and Type III powder (Praxair, USA) – by spray-pyrolysis. The structural and mechanical properties of these powders, the methods of manufacturing as well as the comparative results were reported earlier [15, 16]. The morphological parameters of the powders are shown in the **Table 1**.

Table 1. Morphological parameters of the 1Ce10ScSZ powders [15, 18]

Type of the powder	Size of primary particles, nm	Size of agglomerates, μm	Specific surface, m^2/g
1	11±2	2.3±0,2	48±5
2	73±20	1.5±0,4	12±2
3	64±15	1.3±0,3	5±1

The powders were ball milled in alcohol for 24 h using ZrO_2 media balls and left to dry in air. Afterwards, 10Sc1CeSZ powders were uniaxially pressed at 30 MPa into discs of 20 mm in diameter and 1.5-2 mm thick. 10Sc1CeSZ samples were sintered in the temperature range of 1250-1550 °C for 2 h in air using VK 1600, Linn High Term furnace (Germany). The fractures of the samples were observed by means of a scanning electron microscope (SEM) (Superprobe 733, JEOL).

The electrical impedance of the samples was measured as a function of AC frequency using a Solartron 1260 impedance/gain-phase analyser within the frequency range of 10^{-2}-10^6 Hz at 600 °C in air. For these measurements, the silver paste electrodes were deposited onto the sample surface and sintered.

The resulting impedance diagrams were modelled by means of electrical equivalent circuits (EC), which consisted of two or three parallel *RC*-circuits (depending on the number of the impedance semicircles) and a resistor connected in series. As a result, the model parameters such as the resistances and capacitances of the grains and grain boundaries, Ohmic resistances, and the parameters (α, Θ and β) which reflect the deviation of the impedance spectra from the Debye representation were obtained.

Results

10Sc1CeSZ electrolyte produced from the Type I powder

The impedance spectra of the Type I samples show two or even three semicircles (**Figure 3**) with the two intercepts on the real axis at higher frequencies corresponding to the total ohmic and polarization resistances, respectively. The third semicircle in the low frequency range (<1 Hz) is due to the electrode effects and was observed only for the samples sintered at relatively low temperatures, 1250-1300 °C that had low mechanical strength and were highly porous leading to high ohmic resistances. The second intercept at the intermediate frequencies of 50-100 Hz is related to the blocking of charge carries due to the internal surfaces of the specimens also denoted as intergranular response (grain boundary, GB). The first semicircle at high frequencies (with the peak frequency (PF) of 200-398 kHz was

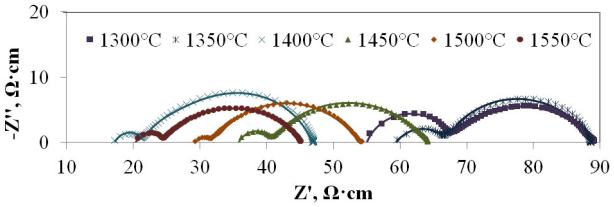

Figure 3. Representative impedance spectra of the Type I samples in regard to their sintering temperature. Dots – experimental data, lines – model approximation.

assigned to the bulk (intragranular) response (grain, G) and the intercept on the real axis in the high frequency range represented the total ohmic resistance.

Based on these and our earlier published results [15], it can be concluded that out of all Type I samples, the sample sintered at 1400 °C has an optimal combination of porosity (32 %), oxygen ionic conductivity, and mechanical behavior .

The grain boundary resistance of the Type I samples is about 30 Ω·cm (**Figure 4**) that does not depend on the sintering temperature. The porosity of the samples decreases from 37 to 21 % with increasing sintering temperature from 1300 to 1550 °C [14, 18], causing increase in the electrical conductivity of ceramics.

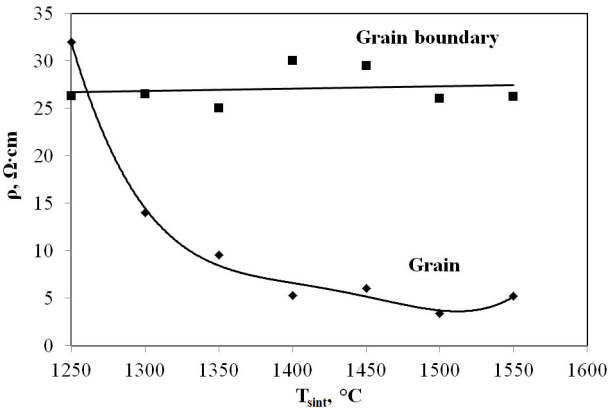

Figure 4. Grain and grain boundary resistances of the Type I samples in regard to their sintering temperature.

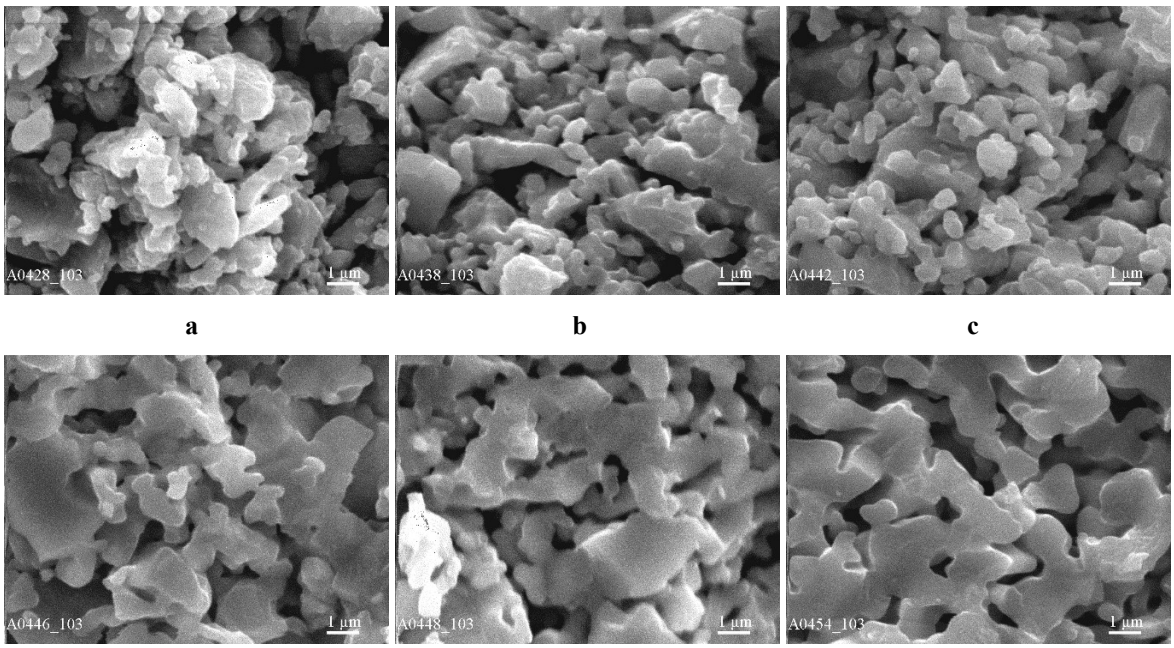

Figure 5. SEM images of the fracture surfaces of the Type I electrolyte sintered at different temperatures: a – 1300 °C; b – 1350 °C; c – 1400 °C; d – 1450 °C; e – 1500 °C; and f – 1550 °C.

The results of the secondary ion mass spectroscopy showed [15] that the surface layer of Type I particles has a large amount of contaminants – Al^{3+}, Si^{4+} and K^{+}, which are known as elements decreasing the ionic conductivity [3, 5, 16]. The grain resistance of the Type I samples is equal to 14 Ω·cm and 9.5 Ω·cm at 1300 and 1350 °C sintering temperatures, respectively (**Figure 4**), and further temperature increase to 1400-1500 °C decreases it to ~ 5 Ω·cm. In contrast to Types II and III, the initial agglomerates in the Type I powder are not uniform which causes densification of Type I disks (**Figure 5**). These results are inversely proportional to the resistance of the grain size at T_{sint}=1300-1350 °C and maintain almost constant resistance at higher sintering temperatures.

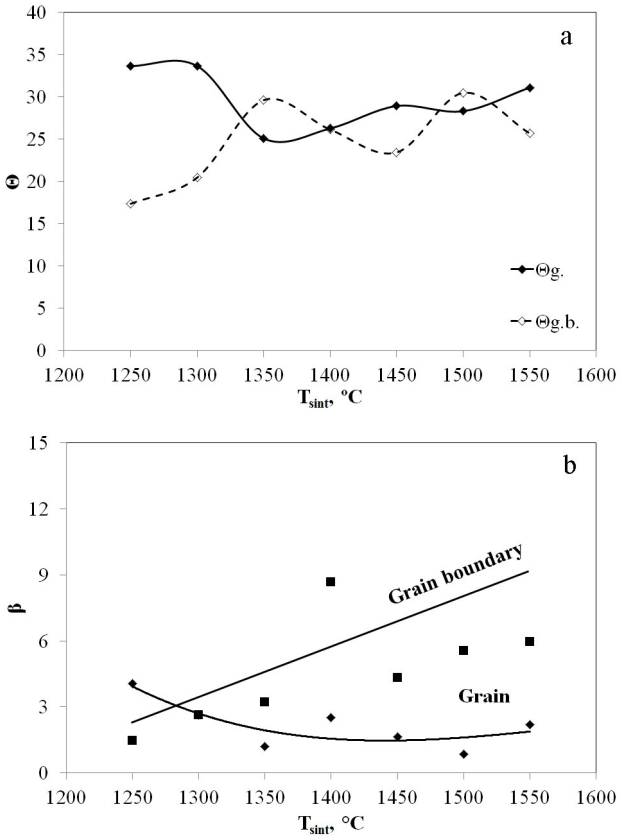

Figure 6. The depression angles Θ and β of the grain boundary (LF) and the grain (HF) components semicircles on the impedance diagrams of the Type I samples in regard to their sintering temperature.

It should be noted that the values of Θ=20.5-30.5° and β<8.7° (**Figure 6**) indicates that the dielectric response of the Type I ceramics obtained at 1300-1550 °C can be described by the Cole-Cole model.

10Sc1CeSZ electrolyte produced from the Type II powder

All Type II 10Sc1CeSZ electrolytes have only one semicircle indicating the grain boundary resistance (GB) in the frequency range of 50-79 Hz (**Figure 7**). Furthermore, the Type II samples have the highest total ionic conductivity due to near zero grain resistance. The grain boundary resistance of the samples obtained at 1300-1350 °C is about 30 Ω·cm, slightly decreases at 1400 °C, and drops twice as much at 1450-1500 °C (**Figure 8**).

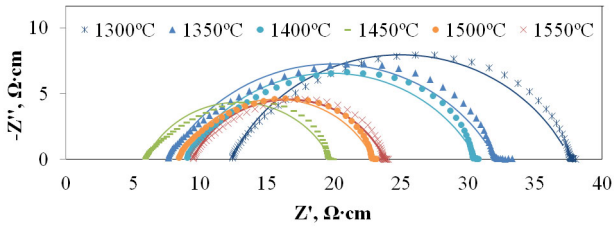

Figure 7. Representative impedance spectra of the Type II samples in regard to their sintering temperature.

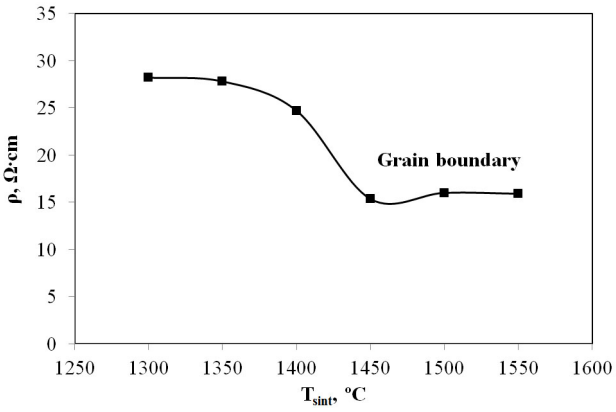

Figure 8. Grain and grain boundary resistances of the Type II samples in regard to their sintering temperature.

The relevant changes are observed in mechanical strength that drops abruptly by more than half.

The nanocracks related to subgrain boundaries disappear as relevant fractographical mark of the interaction between the cleavage cracks and the subgranular interfaces [13, 15]. These complex properties may indicate that in the Type II electrolyte, the sintering at 1350-1400 °C results in a full dissolution of initial particle boundaries, which play a role of subgrain boundaries and are observed as a fractographical fragmentation of grains fracture with cleavage (**Figure 9**) and high subgrain boundary resistance (**Figure 8**).

As result of the high purity of the Type II powder (<10^{-3} wt. % of impurities) [15] a considerable grain growth during the sintering process is observed (**Figure 9**). Such behavior can be explained by the weak influence of the initial boundaries of the particles (subgrains) on a grain recrystallization during the sintering process. Due to this, identification of the grain edges (subgrains) is very complicated and the structure fragmentation totally disappears at the sintering temperatures above 1400 °C (**Figure 9**). We assume that the absence of the grain response (explained by the extremely low impurities content and the decrease of the grain boundary resistance of the samples sintered at the temperatures above 1450 °C) is determined by the grain boundaries improvement, for instance, homogenization of the impurities and

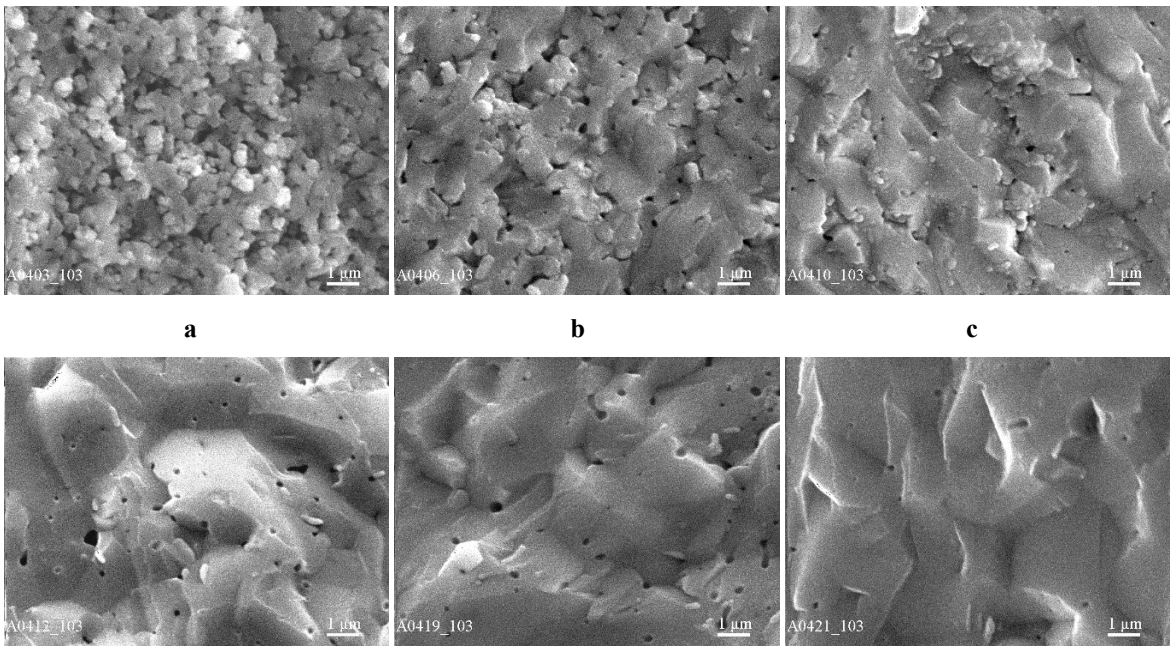

Figure 9. SEM images of fracture surfaces of the Type II electrolyte sintered at temperatures: a – 1300 °C; b – 1350 °C; c – 1400 °C; d – 1450 °C; e – 1500 °C; and f – 1550 °C.

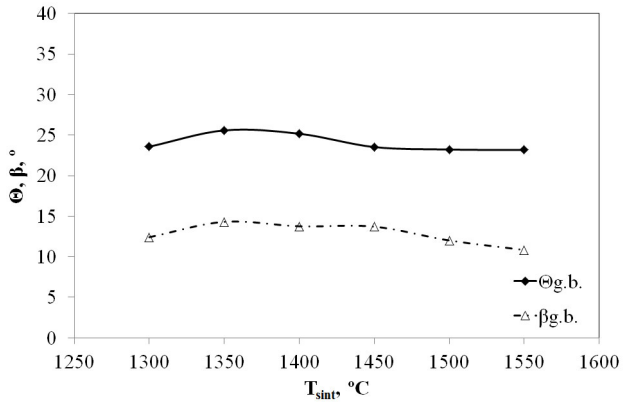

Figure 10. The depression angles Θ and β of the grain boundary (LF) and the grain (HF) components semicircles on the impedance diagrams of Type II samples in regard to their sintering temperature.

structural changes of the grain boundaries.

Parameters Θ=23.2-25.6° and β=10.8-14.3° (**Figure 10**) show that the dielectric response of the samples with only one semicircle on the impedance diagram (the Type II at T_{sint}=1300-1550 °C) is described by the Havriliak-Negami model.

It is known that a deviation from the Debye's model indicates a greater degree of structural heterogeneity 0. The application of the Havriliak-Negami model to the single semicircle may be as an evidence of continuous solid microstructure, where the grain and grain boundary phases cannot be distinguished, i.e., both the bulk of the grains and the intergranular layers have the same chemical composition that may explain the existence of the only one semicircle in a complex plane of Type II 10Sc1CeSZ electrolyte impedance. Thus, the solid phase of the Type II electrolyte is as single-phase in contrast to the Types I where the grain bulk and the phase of the intergranular layers of different origins are detected.

The combination of high ionic conductivity and high ability for densification during the sintering process (residual porosity

less 5 %) at relatively low temperature (1300 °C) [15, 18] makes the Type II material the best candidate for the SOFC electrolyte application.

10Sc1CeSZ electrolyte produced from the Type III powder

The samples of the Type II powder sintered at 1450-1500 °C are characterized by relatively high electrical conductivity (**Figure 11, 12**), high sinterability (residual porosity 13-14 %) and low grain boundary strength revealed as an intergranular fracture (**Figure 13**).

As it is shown in **Figure 11**, the Type III samples sintered at 1300-1400 °C and 1550 °C have two semicircles responsible for the grain boundary (63-316 Hz) and the grain bulk (316-794 Hz) resistances. All other Type III samples demonstrate only one semicircle related to the grain boundary response (126-158 Hz). Here, the grain boundary resistance (30 Ω·cm) is similar to the Type I ceramics and is independent on the sintering temperature. However, taking into account significant densification and porosity decrease from 37 % at T_{sint}=1300 °C to ~0 % at T_{sint}=1550 °C [18], the grain boundary resistance is increasing. This can be explained by the electrical conductivity decrease relevant to the Al^{3+}, Si^{4+}, and K^{+} doping ions found on particle surfaces in this and Type I powders at the first stage of sintering, and the porosity localization along grain boundaries at the second sintering stage [15]. The grain bulk and the ohmic resistances of the ceramics are decreasing with increasing sintering temperatures up to 1450-1500 °C, however, they are increasing at T_{sint}=1550 °C (**Figure 12**). Unlike Type I, the Type III powder consists of equiaxial agglomerates that together with interpartial admixtures accelerate the sintering. An improved contact between the grains (**Figure 13**) at T_{sint}=1450-1500 °C decreases the grain bulk and the ohmic resistances (0 and 15 Ω·cm), respectively. The increase of the grain bulk resistance to 13.5 Ω·cm and ohmic resistance to 20.2 Ω·cm at T_{sint}=1550 °C is related to the intragranular porosity increase (**Figure 13**).

The values of Θ=14.5-36.3° and β<8.1°

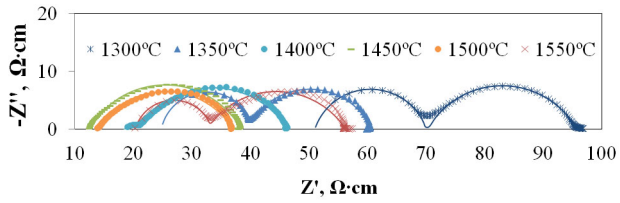

Figure 11. Representative impedance spectra of the Type III samples in regard to their sintering temperature.

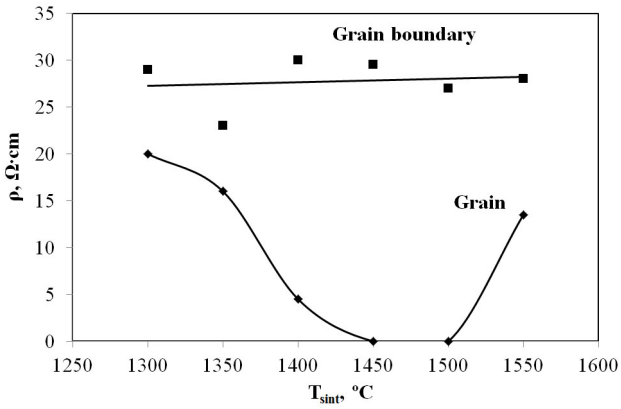

Figure 12. Grain and grain boundary resistances of the Type III samples in regard to their sintering temperature.

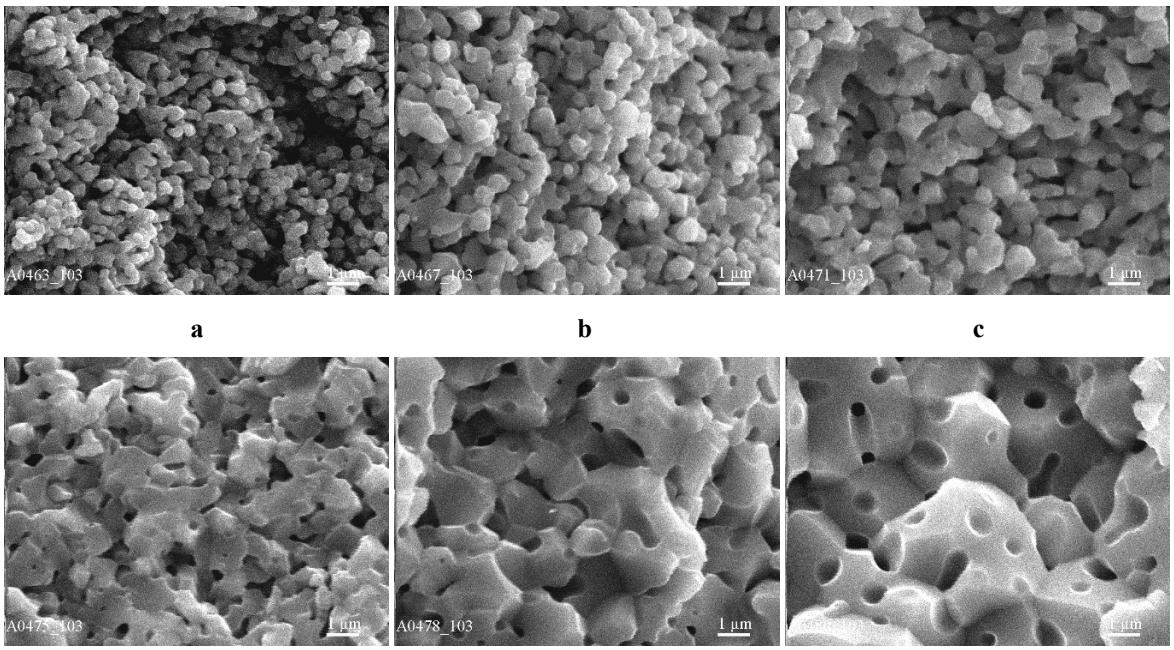

Figure 13. SEM images of fracture surfaces of the type 3 electrolyte sintered at temperatures: a – 1300 °C; b – 1350 °C; c – 1400 °C; d – 1450 °C; e – 1500 °C; f – 1550 °C.

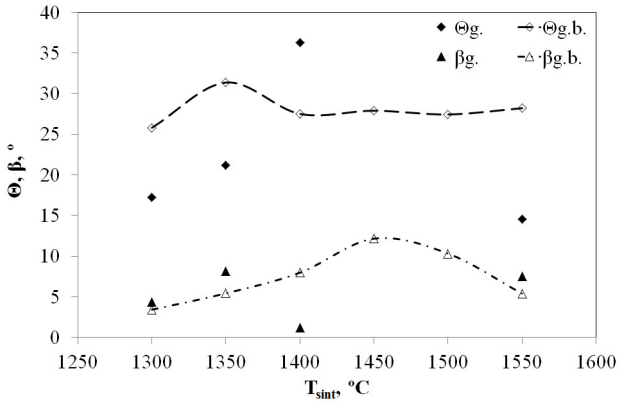

Figure 14. The depression angles Θ and β of the grain boundary (LF) and the grain (HF) components semicircles on the impedance diagrams of Type III samples in regard to their sintering temperature.

indicates that the dielectric response of the Type III samples, obtained at 1300-1400 and 1550°C can be described by the Cole-Cole model (**Figure 14**).

Parameters Θ=27.4-27.9° and β=10.3-12.1° show that the dielectric response of the samples with only one semicircle on the impedance diagram (the Type III at T_{sint}=1450-1500 °C) is described by the Havriliak-Negami model as in previous case.

Discussion

At long term – high temperature processing inherent to ceramic cells, the ordering of polycrystalline electrolyte may result in formation of rather thick intergranular segregating layers similar to those occuring in Type I and III electrolytes and dissolution of subgrains, and growing grains, the boundaries of which remain pure and ordered as interstices between the disoriented grains, that occurs in the Type II electrolyte.

Considering an influence of sintering temperature on the structural parameters and mechanical behavior of 10Sc1CeSZ electrolyte we might conclude [15] that the sintering temperature of 1300-1400 °C is critical for this

material. Namely at this temperatures, the activation energies of grain growth and densification, strengthening or weakening occur. Namely in vicinity of 1300-1400 °C, the strength of the Type II electrolyte is decreased abruptly that is a result of replacement of basic strengthening constituent of the material when subgrains, which boundaries were improved with increasing temperature up to ~1375 °C and dissolved with a further increasing temperature up to ~1400 °C, are replaced abruptly by grains. It should be emphasized here that the grain size does not reveal any evident deviations from the exponential growth that might cause such dramatic changes of the mechanical strength and its decrease from more than 400 to 150 MPa.

The data on the impedance spectroscopy and SEM also indicate two different stages of the traditionally determined boundary or intergranular resistance. During the first stage, till the 1300-1400 °C critical temperatures, the boundary resistance in 10Sc1CeSZ is ~30 Ω·cm that is independent on admixtures and other properties of powder used for the electrolyte production. The improvement of the interpartial or subgranular boundaries is reflected in rapid growth of the electrolyte strength to more than 400 MPa at biaxial bend. High electrical resistance (~30 Ω·cm) of these boundaries points out a weak influence on temperature at this stage of sintering.

During the second stage, at temperatures above 1300-1400 °C, the situation is changed radically. Here, the grains, the boundary structure of which is rather perfect already in order to be easy distinguished fractografically via as both disorientation like in pure Type II electrolyte and admixture segregation additionally like in Types I and III electrolytes. The intergranular constituent of the resistance may be decreased with both abrupt decrease of a specific boundary surface like it happens in Type II electrolyte, and promoting chemical composition of a small amount of impurities segregating along grain boundaries.

In ceramic electrolytes containing a large number of admixtures, the grain boundary response has an unexpected behavior. The temperature increase and the adequate growth of the grain size that depends on amount of admixtures, which are either constraining grain growth like in the Type I electrolyte, or promoting grain growth like in the Type III electrolyte, do not reflect measurably in neither increase, neither decrease of the grain boundary resistance in spite of they influence significantly on the mechanical behavior. At the level of 30 Ω·cm, the difference in neither chemical composition of admixtures and their amounts, nor in their distribution across structure of initial powder particles [13].

Conclusions

It was shown that depending on the chemical purity and morphological parameters

of starting 10Sc1CeSZ powders two general types of ceramics microstructure can be formed during sintering: rather thick intergranular segregating layers similar to those occuring in Type I and III electrolytes and dissolution of subgrains, and growing grains, the boundaries of which remain pure and ordered as interstices between the disoriented grains, that occurs in the Type II electrolyte. It results in two different types of electrical response which determines different applications of the powders.

It was shown that the Type II 10Sc1CeSZ is the best as an SOFC electrolyte because it ensures the highest ionic conductivity resulting from the single-phase homogeneity of the ceramics and close-to-zero resistance of the grain bulk measured at 600 °C.

The Type I 10Sc1CeSZ powder being sintered without any pore formers ensures an optimal combination of high porosity (above 30 %), high electrical conductivity, and mechanical strength which makes this powder an excellent candidate for anode application.

The resistance of intergranular phase is ~30 Ω·cm at all sintering temperatures and does not depend on the type and the amount of admixtures and their distribution across the grains, size of the structural constituents, such as general porosity and, in many cases, sintering temperature and it does not correlate with any fracture micromechanism whereas at significant level of admixture segregations, both cleavage mechanism of grains and brittle intergranular fracture may occur. The resistance of the Type II 10Sc1CeSZ electrolyte abruptly decreases from 30 to 17 Ω·cm when subgrains are replaced by grains abruptly. It occurs at ~1375 °C when the activation energy of numerous thermoactivated processes of powder consolidation is changed, and the mechanical strength decreases abruptly from >400 MPa to ~150 MPa.

As to the grain bulk resistance it can be concluded that in Type I electrolyte, it decreases from 14 to 6 Ω·cm with porosity decrease at 1300-1450 °C and does not depend on structural evolution considering the cleavage fracture mechanism. In Type II electrolyte, the grain body resistance cannot be detected indicating that the electrochemical properties of the grain bodies and their boundaries are the same, and the material is a single phase one. In Type III electrolyte, the resistance decreases from 20 to 5 Ω·cm at decreasing porosity and interpartial fracture mechanism at 1300-1400 °C; it becomes almost zero at mixed fracture mechanisms (1450-1500 °C), and increases to 13 Ω·cm during the recrystallizing grain growth.

Acknowledgements

The authors gratefully acknowledge the American Chemical Society Petroleum Research Fund Project N53614-UR10; the European FP7 and FP6 Projects: NANOMAT-EPC N608906 "Deployment of Socially Beneficial Nano- and Material Technologies in European Partnership Countries", and N020089

"Demonstration of SOFC stack technology for operation at 600 oC (SOFC600)"; NATO, the "Science for Peace" project N980878 "Solid Oxide Fuel Cells for Energy Security", the National Academy of Science of Ukraine, Projects "Structural Fundamentals of Materials for Zirconia Ceramic Fuel Cells", and "SOFC structural optimization based on consideration of interdiffusion at manufacturing and operation" for their financial support.

References

[1] Badwal SPS. Zirconia-based solid electrolytes: microstructure, stability and ionic conductivity. Solid State Ionics. 1992;52:23-32.

[2] Wang Z, Cheng M, Dong Y, Zhang M, Zhang H. Anode-supported SOFC with 1Ce10ScZr modified cathode/electrolyte interface. J. Power Sources. 2006;156:306–310.

[3] Stafford RJ, Rothman SJ, Routbort JL. Effect of dopant size on the ionic conductivity of cubic stabilized ZrO_2. Solid State Ionics. 1989;37:67-72.

[4] Liu M, He CR, Wang WG, Wang JX. Synthesis and characterization of 10Sc1CeSZ powders prepared by a solid–liquid method for electrolyte-supported solid oxide fuel cells. Ceram. Int. 2014;40(4):5441-5446.

[5] Haering C, Roosen A, Schichl H, Schnoller M. Degradation of the electrical conductivity in stabilized zirconia system. Part II: Scandia-stabilized zirconia. Solid State Ionics. 2005;176:261-268.

[6] Liu M, He C, Wang J. Investigation of $(CeO_2)_x(Sc_2O_3)_{(0.11-x)}(ZrO_2)_{0.89}$ (x=0.01- .10) electrolyte material for intermediate-temperature solid oxide fuel cells. J. Alloy. Compd. 2010;502:319–323.

[7] Badwal SPS, Drennan J. Microstructure/conductivity relationship in the scandia–zirconia system. Solid State Ionics. 1992;53–56:769–776.

[8] Mizutani Y, Tamura M, Kawai M. Development of high-performance electrolyte in SOFC. Solid State Ionics. 1994;72:271–275.

[9] Ruh R, Garrett HJ, Domagala RF. The system zirconia-scandia. J. Am. Ceram. Soc. 1977;60:399–403.

[10] Tu H, Liu X, Yu Q. Synthesis and Characterization of Scandia ceria stabilized zirconia powders prepared by polymeric precursor method for integration into anode-supported solid oxide fuel cells. J. Power Sources. 2011;196:3109–3113.

[11] Fonseca FC, Mucillo R. Impedance spectroscopy analysis of percolation in (yttria-stabilized zirconia)-yttria ceramic composites. Solid State Ionics. 2004;166:157-165.

[12] Alim MA, Bissel SR, Mobasher AA. Analysis of the AC electrical data in the Davidson-Cole dielectric representation. Phys. B. 2008;403:3040-3053.

[13] Mastroianni I, Poorteman M, Moortgat G, Gambier F. Impedance spectroscopy for nondestructive characterization of ceramic compacts Key Eng. Mat. 2004;264-268:113-116.

[14] Brodnikovska I. Electronics and Communications. 2015;20(1)(84);9-17.

[15] Vasylyev OD, Smirnova AL, Brychevskyi MM, Brodnikovskyi IM, Firstov SO, Vereschak VG, Akimov GY, Komysa YO, Irvine JTS, Savaniu CD, Sadykov VA, Kosacki I. Structural, Mechanical and Electrochemical Properties of Ceria Doped Scandia stabilized Zirconia. Material Science of Nanostructures. 2011;1:70-80.

[16] Grzonka J, Vereshchak V, Shevchenko O. Vasylyev O, Kurzydłowski KJ. Characterization of Sc_2O_3&CeO_2—Stabilized ZrO_2 powders via co-precipitation or hydrothermal synthesis. Microsc. Microanal. 2013;19(5):29-32.

[17] Guo CX, Wang JX, He CR. Effect of alumina on the properties of ceria and scandia co-doped zirconia for electrolyte-supported SOFC. Ceram. Int. 2013;39:9575–9582.

[18] Brychevskyi M, Vasylyev O, Brodnikovskyi Ye. Influence of sintering temperature on structure and mechanical behavior of 1Ce10ScSZ ceramics. Electron microscopy and strength of materials. 2013;19:169-183 (in Ukrainian).